



HAL
open science

Development of a Large-Scale Environmental Chamber for Investigating Soil Water Evaporation

Weikang Song, Yu-Jun Cui, Anh Minh A.M. Tang, Wenqi Ding

► **To cite this version:**

Weikang Song, Yu-Jun Cui, Anh Minh A.M. Tang, Wenqi Ding. Development of a Large-Scale Environmental Chamber for Investigating Soil Water Evaporation. *Geotechnical Testing Journal*, 2013, 36 (6), pp.847-857. 10.1520/GTJ20120142 . hal-00926880

HAL Id: hal-00926880

<https://enpc.hal.science/hal-00926880>

Submitted on 25 Apr 2018

HAL is a multi-disciplinary open access archive for the deposit and dissemination of scientific research documents, whether they are published or not. The documents may come from teaching and research institutions in France or abroad, or from public or private research centers.

L'archive ouverte pluridisciplinaire **HAL**, est destinée au dépôt et à la diffusion de documents scientifiques de niveau recherche, publiés ou non, émanant des établissements d'enseignement et de recherche français ou étrangers, des laboratoires publics ou privés.

1 **Development of a Large-Scale Environmental Chamber for**
2 **Investigating Soil Water Evaporation**

3
4 Wei-Kang SONG^{1,2}, Yu-Jun CUI^{1,2}, Anh Minh TANG², Wen-Qi DING¹
5

6 1 Department of Geotechnical Engineering, Tongji University, Shanghai, China

7 2 Université Paris-Est, Laboratoire Navier (UMR 8205 CNRS-IFSTTAR-ENPC), Ecole des
8 Ponts ParisTech, 6-8, av. Blaise. Pascal, 77455 Marne-la-Vallée, France

9
10 **Corresponding Author:**

11 Prof. Yu-Jun CUI

12 Ecole des Ponts ParisTech

13 6-8 av. Blaise Pascal, Cité Descartes, Champs-sur-Marne

14 F-77455 MARNE LA VALLEE

15 France

16
17 Telephone : +33 1 64 15 35 50

18 Fax : +33 1 64 15 35 62

19 E-mail : yujun.cui@enpc.fr
20

21 **ABSTRACT:** A large-scale environmental chamber was developed to study the soil water
22 evaporation mechanisms. A large soil specimen (300 mm high, 800 mm large and 1000 mm
23 long) was used, allowing sensors to be installed with minimal effect on the soil hydraulic
24 properties. Sensors for measuring soil suction, temperature and volumetric water content were
25 either buried inside the soil specimen or installed on the chamber's wall at various locations.
26 Other sensors for monitoring air temperature, relative humidity, air flow rate and soil surface
27 temperature were installed at different locations above the soil surface. Meanwhile, various
28 atmosphere conditions were controlled by an air supply system and a steady water table at the
29 bottom of soil was set through a big water tank. Fontainebleau sand was studied and it was
30 compacted in the chamber in layers. After saturation, an 11.5-day evaporation test was
31 performed. The results obtained were presented in terms of evolutions of suction, volumetric
32 water content, air relative humidity and soil/air temperature. The data of air relative humidity
33 and air temperature were further used for determining the actual evaporation rate; the data of
34 soil volumetric water content and soil suction were used for determining the soil water
35 retention curve. The quality of the results obtained showed the performance of the
36 environmental chamber developed. In addition, these results can be further analyzed for
37 theoretical and numerical developments involving soil water evaporation.

38

39 **KEYWORDS:** environmental chamber; Fontainebleau sand; soil water evaporation; soil
40 suction at surface

41 **Introduction**

42 Soil water evaporation is an essential component in the land surface energy balance (Daamen
43 and Simmonds 1996). Water is lost from soil during evaporation, thereby influencing the soil
44 behavior, especially for clayey soils. In the field of agronomy, water loss due to evaporation
45 can significantly affect crops in the planting and germination periods (Lal and Shukla 2004);
46 in the geotechnical field, considerable water loss (e.g., drought) can induce significant soil
47 volume changes, thereby damaging buildings and other infrastructures (e.g., Cui and Zornberg
48 2008; Corti et al. 2009; Corti et al. 2011). Furthermore, soil water evaporation also affects the
49 design, selection and assessment of soil cover for landfill and mining application (e.g., Wilson
50 et al. 1994; Yanful and Choo 1997; Yanful et al. 2003). Therefore, it is important to better
51 understand the soil water loss process during evaporation.

52

53 In order to estimate soil water evaporation, various devices and methods have been developed.
54 Evaporation pan is usually used in the field for the measurement of free water evaporation
55 that is considered as potential soil water evaporation (e.g., Blight 1997; Singh and Xu 1997;
56 Fu et al. 2004; Fu et al. 2009; Li and Zhang 2011). For soil water evaporation investigation,
57 several un-complex devices have also been developed. For instance, a circular pan with 300
58 mm in diameter but different heights and filled with compacted soil was developed by Kondo
59 et al. (1990, 1992), a soil column drying test device (Wilson et al. 1994) and a pan with 258
60 mm in diameter and 74 mm in height and filled with thin enough soil sample by Wilson et al.
61 (1997). The evaporation rate was obtained directly by weighing these devices over time.
62 Furthermore, the devices developed by Kondo et al. (1992) and Wilson et al. (1994) allow

63 continuously monitoring the soil temperatures at various depths. For the water content profile,
64 it was obtained only once by oven-drying at the end of experiment conducted by Kondo et al.
65 (1992) while the evolution of it during evaporation can be obtained by direct measurement via
66 sampling ports at various depths in the test performed by Wilson et al. (1994). More recently,
67 McCartney and Zornberg (2010) developed a large soil column evaporation system based on
68 the infiltration test devices developed by Stormont and Anderson (1999), Bathurst et al. (2007)
69 and Bathurst et al. (2009), to investigate both the evaporation and infiltration processes. Their
70 system allows the simultaneous measurements of soil temperature, water content/suction.
71 Following the similar measurement principle that water evaporation approximately equals the
72 mass loss of soil, weighing lysimeter was developed that allows direct measurement of
73 evaporation as changes in total mass of soil (e.g., Benson et al. 2001; Benli et al. 2006). In
74 order to make the in-situ measurement simpler and more accurate, micro-lysimeter are used
75 (e.g., Boast and Robertson 1982; Plauborg 1995; Wang and Simmonds 1997; Qiu et al. 1998;
76 Bonachela et al. 1999; Liu et al. 2002). Micro-lysimeter can also be combined with water
77 content sensors like TDR (time domain reflectometry) for water evaporation monitoring
78 (Wythers et al. 1999).

79

80 A better control of atmospheric conditions is obviously essential in investigating soil water
81 evaporation mechanisms. In this regard, the wind tunnel system is a good example. Typically,
82 this system allows not only the control of wind velocity and solar radiation, but also the
83 monitoring of air temperature and relative humidity (e.g., Yamanaka et al. 1997; Komatsu
84 2003; Yamanaka et al. 2004; Yuge et al. 2005; Wang 2006). This system can be used in

85 combination with the experimental devices mentioned above like pan (e.g., Komatsu 2003),
86 soil tank (e.g., Wang 2006), weighing lysimeter (e.g., Yamanaka et al. 1997; Yamanaka et al.
87 2004) and micro-lysimeter (e.g., Yuge et al. 2005). Furthermore, if some sensors are used for
88 soil temperature, suction and volumetric water content monitoring, this system allows a
89 comprehensive monitoring of parameters for studying soil water evaporation (e.g., Yamanaka
90 et al. 1997; Yamanaka et al. 2004).

91

92 Another commonly used system is the environmental chamber. A fast air circulation box was
93 developed by Kohsiek (1981) with the simulation of wind. It is a useful chamber for the
94 measurement of stomatal resistance of grass. After some minor adjustments and equipment of
95 a fast dry and wet bulb thermocouple and a thermal infrared radiometer, this box was then
96 used for soil surface resistance investigation (van de Griend and Owe 1994). Furthermore,
97 based on the principle that changes in absolute humidity at inlet and outlet of the
98 environmental chamber is due to the soil water evaporation, Mohamed et al. (2000) developed
99 a new chamber for predicting the solute transfer in unsaturated sand due to water evaporation,
100 and Aluwihare and Watanabe (2003) developed a chamber to study the surface resistance of
101 bare soil. On the whole, these chambers focus on the control atmosphere conditions, such as
102 wind velocity, relative humidity, temperature etc., but rarely account for the soil parameters
103 such as water content and suction. On the other hand, Yanful and Choo (1997) performed an
104 evaporation experiment on a compacted soil using cylindrical columns placed in an
105 environmental chamber. This chamber can control air temperature and relative humidity and
106 measure soil temperature and water content at different depths during evaporation. However,

107 the soil mass, temperature and water content measurements should be done outside the
108 chamber, the measurements being not instantaneous and continuous. Tang et al. (2009)
109 developed a large-scale infiltration tank allowing instantaneous monitoring of soil water
110 content, temperature and suction during evaporation (Ta et al. 2010; Cui et al. 2013).

111
112 The various devices and methods mentioned above show that the large-scale environmental
113 chamber is a good tool for investigating soil water evaporation in the laboratory. Compared to
114 the wind tunnel system, the environmental chamber is less expensive and easier to operate but
115 can provide rich data involving both air and soil parameters. Moreover, it has the same
116 function as the combination of the wind tunnel and lysimeter. However, most existing
117 environmental chambers only have a good performance in controlling air conditions, the soil
118 being hardly taken into account (e.g., Kohsiek 1981; Van de Griend and Owe 1994;
119 Aluwilhare and Watanabe 2003). In addition, the relationship between actual evaporation and
120 soil suction or water content near the soil surface was rarely studied.

121
122 In this study, a large scale environmental chamber (1000 mm long, 800 mm wide and 895 mm
123 high) was developed for studying soil water evaporation. An 11.5-day evaporation test was
124 performed on the Fontainebleau sand. Various sensors were buried in the soil or installed on
125 the wall of chamber at different depths, allowing monitoring of soil temperature, suction,
126 volumetric water content, in addition to the air temperature and relative humidity. The
127 recorded data were further analyzed to determine the actual evaporation rate and soil water

128 retention curve. Note that this study focuses on soil water evaporation. To some extent, it
129 corresponds to an extension of unsaturated soil mechanics.

130

131 **Experimental Setup**

132 The experimental setup consists of an environmental chamber, a wind supply unit, an air
133 collection unit, a water supply unit and a data logging system. A sketch of this system is
134 shown in Fig. 1. Schematic views of the environmental chamber are presented in Fig. 2 and a
135 photograph is shown in Fig. 3. The chamber includes the main body, the ventilation part, the
136 soil column part, the water drainage layer and an acrylic chamber cover of 8 mm thick.

137

138 The main body is an acrylic transparent chamber fixed on a base. The chamber consists of
139 four acrylic plates mounted together by epoxy glue. The chamber has a wall of 20 mm thick,
140 an internal width of 800 mm and an internal length of 1000 mm (Fig. 2(a)). Silicon glue was
141 used to seal the joints in the four corners for preventing any leakage of air or water.

142

143 The soil column was prepared by compaction. The sensors measuring volumetric water
144 content and soil temperature were installed at various depths during the compaction. The
145 drainage layer was a compacted gravel (diameter: 2 - 4 mm) layer of 15 mm thick and
146 sandwiched between two layers of geotextile of 1 mm thick (Fig. 2(b)). Two outlets were
147 prepared at the bottom of the drainage layer for soil saturation, drainage and water supply.

148

149 The details of the sensors used are presented in Table 1 and their locations are shown in Fig.

150 2(b). These sensors were installed at different monitoring points in both the soil column and
151 air. The volumetric water content sensors, namely ThetaProbe, were buried at different depths
152 (i.e., 25 mm, 40 mm, 55 mm, 125 mm and 225 mm below the soil surface). Four
153 high-capacity tensiometers of 1.5 MPa working suction (Cui et al. 2008, Tang et al. 2010)
154 were installed on two sides of the wall at various depths (i.e., 25 mm, 77 mm, 173 mm and
155 276 mm below the soil surface). One tensiometer was placed near the surface of soil (10 mm
156 below the soil surface in order to ensure the good contact between the tensiometer and soil).
157 Six soil temperature sensors (PT1000) were set every 50 mm along the soil column. Moreover,
158 an infrared thermometer was fixed at the cover to measure the soil surface temperature. Six
159 T3111 transmitters were mounted inside and outside the chamber. Two of them were placed at
160 the air inlet and outlet. For the other four sensors, one was fixed on the chamber's wall in the
161 middle from the soil surface to the cover of chamber (i.e., 275-mm height); the second one
162 was mounted outside the chamber for monitoring the laboratory relative humidity; the last
163 two sensors were placed on the soil surface and at 50 mm above the soil surface, respectively.
164 The thermistors that allow the measurement of air temperature were fixed at different
165 elevations along one side of the wall in the ventilation part.

166

167 The wind supply unit (see Fig. 1) was used for controlling the atmospheric conditions such as
168 air temperature and air flow rate. This system consists of five parts: (1) high-pressure
169 compressed air source; (2) air flow rate measurement unit; (3) air heating unit; (4) relative
170 humidity and temperature measurement unit; and (5) air distributor. The compressed air
171 source corresponds to the common laboratory compressed air system. The air flow rate is

172 controlled by a valve and is monitored by a flowmeter. The air heating unit consists of heating
173 hoses and temperature regulator. This unit can heat the air to a temperature up to 250 °C. The
174 unit measuring air relative humidity and temperature is equipped with a rigid plastic cell in
175 which a T3111 transmitter is inserted. The air distributor is a metal tube on which eight holes
176 of 8.4 mm in diameter are drilled along the length of tube with a spacing of 100 mm.

177

178 The air collection unit, assembled on the opposite wall to the air distributor, is half of a
179 polyvinyl chloride cubic box of 755 mm long, 30 mm large and 100 mm high. This unit
180 collects the air from the chamber and a T3111 transmitter inside measures both the relative
181 humidity and temperature of air. A total of five holes of 25 mm diameter in the wall of
182 chamber enable the air to enter the collection unit.

183

184 The water supply unit for the chamber consists of a plastic water tank and a water table
185 survey tube. The water tank supplies water to the chamber and the water level inside the tank
186 is kept the same as the water table in the chamber (bottom of chamber in this study). The
187 water table survey tube is a glass tube with marks and connected to the water tank. Thereby,
188 any change of water table in the chamber can be detected. When the water table lowers down
189 due to soil evaporation in the chamber, more water is added to the tank to keep a constant
190 water table. The quantity of water added is also recorded.

191

192 **Material and Experimental Procedure**

193 The soil used for this experiment is the Fontainebleau sand. It is a natural, fine, white

194 siliceous sand. Its specific gravity, maximum density and minimum density are 2.64, 1.39
195 Mg/m^3 , and 1.75 Mg/m^3 , respectively. The effective grain size D_{10} is 0.14 and the coefficient
196 of uniformity, $C_u = D_{60}/D_{10}$, is 1.6 (see Delfosse-Ribay et al. 2004).

197

198 For the compaction of sand, 68 kg of dry sand was first poured into the tank and compacted
199 manually to have a layer of 50 mm thick, corresponding to a dry density of 1.7 Mg/m^3 . This
200 procedure of compaction was repeated until reaching the total height of 300 mm.

201

202 During compaction, the installation of sensors was performed. The PT1000 sensors measuring
203 the soil temperature were buried above each layer (the spacing was then 50 mm). For the
204 ThetaProbe sensors, two were inserted in the sand during the compaction and the others were
205 buried in the first 60 mm below the soil surface after the soil saturation. For burying the
206 ThetaProbe sensors, a hole having similar dimensions as the sensor was created manually at
207 the defined level, and then the sensor was placed horizontally in the hole by inserting the four
208 steel guides inside the soil. The hole was finally filled and manually compacted with a
209 previously determined quantity of sand in order to ensure the same dry density. This
210 procedure aimed at minimizing the effect of sensors installation on the soil density as
211 described by Tang et al. (2009).

212

213 After the soil compaction and sensors installation, the soil column was saturated through the
214 water tank connected to the bottom of chamber. After saturation, the water level in the tank
215 was lowered to a depth of 280 mm, i.e., the bottom of soil column. The installation of

216 tensiometers was conducted during this water drainage progress. Furthermore, a relative
 217 humidity sensor on the soil surface was installed and the cover of chamber was sealed by
 218 silicon to ensure the air-tightness.

219

220 As far as the evaporation rate calculation is concerned, the basic principle is the calculation of
 221 the variation of air absolute humidity at the inlet and outlet of chamber. This method is
 222 described as follows (Mohamed et al. 2000; Aluwihare and Watanabe 2003):

223 The evaporation rate is calculated by the following expression:

$$224 \quad E_a = 86400 \frac{Q(H_{a_outlet} - H_{a_inlet})}{\rho_w A} \quad (1)$$

225 where E_a is the actual evaporation rate (mm/day), H_{a_outlet} is the absolute humidity at outlet
 226 (Mg/m^3), H_{a_inlet} is the absolute humidity at inlet (Mg/m^3), Q is the air flow rate through the
 227 chamber (L/s), ρ_w is the density of water (Mg/m^3) and A is the area of soil evaporation surface
 228 in the chamber (m^2).

229 The absolute humidity (H_a) is calculated as follows:

$$230 \quad H_a = \frac{0.622 p_a}{1000RT_a} \quad (2)$$

$$231 \quad e_a = \frac{e_{sat} H_r}{100} \quad (3)$$

$$232 \quad e_{sat} = 101325 \exp\left(\frac{17.63 - 185}{T_a} - \frac{9760}{T_a^2} - 0.644\right) \quad (4)$$

$$233 \quad t_{R_a} = 1 - \frac{373.1}{T_a} \quad (5)$$

234 where e_a is the vapor pressure (Pa); T_a is the air temperature (K); R is the gas constant (287.04
 235 $\text{J}\cdot\text{kg}^{-1}\text{K}^{-1}$); e_{sat} is the saturated vapor pressure (Pa); H_r is the air relative humidity (%); and
 236 0.622 is the ratio of the molecular weights of water and dry air.

237

238 In this study, the air flow rate was maintained at 172 L/min and the heating tube temperature
239 was 200 °C which corresponds to a temperature of 47 °C at the inlet of chamber.

240

241 **Experimental Results**

242

243 The air supply unit provided compressed hot air to the chamber at a rate of 172 ± 5 L/min.

244 Figure 4 shows changes of air temperature over time. The values in the chamber increase

245 during evaporation within a range from 24 °C to 32 °C. The shapes of the curves are similar

246 showing a slight increase during the first six days and a quick increase during the last six days.

247 The values are very similar when the locations are above 185 mm. Note that the sensors at

248 275 mm, 380 mm and 465 mm above the soil surface give similar temperatures and they are

249 therefore termed as “other sensors” in Fig. 4.

250

251 The changes of air temperatures at the inlet, outlet of chamber and in the laboratory are shown

252 in Fig. 5. The value at the inlet is 47 ± 3 °C, whereas the value at the outlet is lower and is

253 increasing during the test from 25 °C to 30 °C. The laboratory room temperature varies from

254 20 °C to 24 °C and is lower than at the inlet and outlet.

255

256 The evolution of soil temperature is shown in Fig. 6. It is observed that the values increase

257 slightly during the first six days but significantly during the last six days. The highest

258 temperature is at the soil surface. In the deeper levels (25, 40, 55, 125 and 225-mm depths)

259 corresponding to “other sensors” in this figure, the values are very close and increase from

260 18 °C to 25 °C. However, the soil surface temperature increases from 19 °C to 30 °C. Note
261 that the surface temperature is not available for the period of $t = 2 - 3$ days due to some
262 technical problems.

263

264 All the temperature data recorded are used to plot the air-soil temperature profiles (Fig. 7).
265 For the air temperature, the highest value appears at the elevation corresponding to the
266 location of air distributor (300 mm above the soil surface), the temperature in the zone close
267 to the cover being lower due to the influence of laboratory room temperature. Regarding the
268 soil temperature changes, a sharp temperature decrease can be observed in the near soil
269 surface zone. The air temperature is significantly higher than the soil temperature.
270 Furthermore, the temperature gradient above the soil surface (in the zone from 80 mm above
271 the soil surface to the soil surface) decreases progressively over time while the gradient
272 between the soil surface and 25-mm depth increases. The soil temperatures in deeper zone
273 (from 25-mm depth to the soil bottom) are quite similar with a difference less than 0.5 °C.

274

275 The changes of air relative humidity are shown in Fig. 8. The values in the chamber decrease
276 from 67.4 % to 23.8 % in the zone near the soil surface and from 35.4 % to 12.4 % at the
277 outlet, while the values at the inlet are very low and nearly constant. On the whole, the
278 variations of relative humidity (except that at the inlet of chamber and in the laboratory) can
279 be divided into two parts: during the first six days, the relative humidity declines at a low rate;
280 then it drops in the next six days. The value at the soil surface was higher than in other
281 locations. The relative humidity in the laboratory shows a large fluctuation, from 19.7 % to

282 40.5 %, but this does not affect the values measured in the chamber.

283

284 The changes of volumetric water content are shown in Fig. 9. The volumetric water content at
285 60 mm below the soil surface decreases from 25.4 % to 7.1 % at 25-mm depth and from
286 31.9 % to 12.3 % at 55-mm depth. In the deeper locations, i.e., at 125 and 225-mm depths,
287 there are no changes before $t = 7$ days. The value remains unchanged at 225-mm depth during
288 the whole test while the value at 125-mm depth starts to change from $t = 7$ days. As far as the
289 first 60-mm layer near the soil surface is concerned, the variation can be divided into two
290 parts: at the beginning, the water content decreases quickly in the first six day and then
291 decreases slowly and reaches a stabilization state at end of the test.

292

293 The profiles of volumetric water content and the contour map are shown in Fig. 10. The
294 profiles in Fig. 10(a) show a clear water loss process during evaporation. It can be noted that
295 the gradient of water content between the three points at 25, 40, and 55-mm depths
296 respectively is constant and equal to 0.2 %/mm. This gradient is also the maximum for the
297 whole depth. Similar linear gradient of water content can be observed from 25-mm to
298 225-mm depth at end of the test ($t = 11.5$ days). The contour map allows the visualization of
299 the drying front over time (see Fig. 10(b)). For instance, the point having a water content of
300 30 % is at 50-mm depth at the beginning; this point goes down quickly and reaches the first
301 stabilization stage at 120-mm depth after $t = 2$ days. It starts to increase again only at $t = 7$
302 days. This means that from $t = 2$ days to $t = 7$ days, the water loss in the soil takes place only
303 in the zone from the soil surface to 120-mm depth.

304

305 The evolution of soil matric suction is presented in Fig. 11. All the suction values at various
306 locations are increasing with the water loss. Near the soil surface, the soil matric suction
307 increases gradually from 14 kPa at $t = 0$ day to 46 kPa at $t = 8$ days. It increases quickly and
308 reaches the limit of the sensor (i.e., 1.5 MPa) a few hours later. For the soil suction at other
309 depths, the value at 77-mm depth is higher than at 173-mm depth but the difference is small.
310 The lowest suction is at 276-mm depth. The profile of soil suction is presented in Fig. 12. A
311 clear and sharp suction gradient is observed in the zone from the soil surface to 77-mm depth.
312 This gradient is increasing over time: it increases from 0.13 kPa/mm at the beginning to 0.46
313 kPa/mm at $t = 8$ days.

314

315 The simultaneous measurement of suction and volumetric water content at various depths
316 during the drying process allows determination of the soil water retention curve, as shown in
317 Fig. 13. For each level of soil suction measurement (see Fig. 11), the corresponding
318 volumetric water content is determined based on the volumetric water content profiles shown
319 in Fig. 10(a); the volumetric water content at the soil surface is extrapolated by taking a
320 constant water content gradient of 0.2 %/mm in the near surface zone. An air entry value of 7
321 kPa can be estimated in Fig. 13. It is also possible to use the model proposed by Fredlund and
322 Xing (1994) to fit the water retention curve:

323
$$\theta_w = \theta_r + \frac{\theta_s - \theta_r}{\left\{ \ln \left[e + (\psi / a)^n \right] \right\}^m} \quad (6)$$

324 where θ_w is the volumetric water content (%); θ_s is the volumetric water content in saturated
325 state ($\theta_s = 35.6\%$); θ_r is the residual volumetric water content ($\theta_r = 4.4\%$); ψ is the matric

326 suction (kPa); e is the base of natural logarithm ($e = 2.71828$); a , n and m are fitting
327 parameters. The fitting curve shown in Fig. 13 corresponds to $a = 45.74$, $n = 1.9$ and $m =$
328 15.2.

329

330 The actual evaporation rate determined following Eq 1 and the evolution of suction gradient
331 between soil surface and 77-mm depth are plotted in Fig. 14. Regarding the evolution of
332 evaporation rate, three phases can be identified: from $t = 0$ to $t = 6$ days, the rate decreases
333 slightly from 2.3 mm/day to 2.0 mm/day; in the next 4 days, it decreases rapidly from 2.0
334 mm/day to 0.9 mm/day; after $t = 10$ days, the value decreases slowly, from 0.9 mm/day to 0.8
335 mm/day in 1.5 days. As far as the suction gradient is concerned, it increases slowly from the
336 initiation of evaporation to $t = 8$ days, and then quickly reaches 4.8 kPa/mm at $t = 8.5$ days.
337 Interestingly, the high suction gradient corresponds to the significant decrease of evaporation
338 ratio, indicating the increase of soil resistance to evaporation by suction increase.

339

340 As far as the cumulative evaporation is concerned, the calculation results of two different
341 methods are presented in Fig. 15. Method 1 corresponds to direct calculation according to the
342 actual evaporation rate - the results are shown in solid line. Method 2 corresponds to indirect
343 determination by summing up the quantity of water infiltrated and the quantity from changes
344 of volumetric water content - the results are plotted in dashed line. Note that the quantity of
345 water infiltrated is calculated through the mass of water flowing out of the water tank divided
346 by the soil evaporation surface, i.e., 1000 by 800 mm. The changes of volumetric water
347 content are determined by considering the volumetric water content profiles shown in Fig.

348 10(a). The cumulative evaporation derived from Method 1 increases linearly over time but
349 slows down after six days due to the decrease of evaporation rate. A total of 20.4 mm water is
350 evaporated at the end of test. The cumulative quantity of water infiltrated increases following
351 a linear function with time from the beginning to $t = 3.7$ days; it starts to slow down after four
352 days. A total of 7.7 mm of water enter the chamber at the end of test. The cumulative quantity
353 from changes of water content profiles increases during the test and reaches 24.5 mm at the
354 end. It appears clearly that Method 2 gives higher cumulative evaporation than by Method 1,
355 32.2 mm against 20.4 mm.

356

357 **Discussion**

358 The environmental chamber system is a promising method for soil water evaporation
359 investigation. As mentioned before, a fast air circulation box was developed by Kohsiek
360 (1981) and a similar facility was used by van de Griend and Owe (1994), focusing on the
361 reproduction of wind. Furthermore, the chamber built by Mohamed et al. (2000) and the
362 chamber system used by Aluwihare and Watanabe (2003) had a good control and
363 measurement of air conditions but not the soil conditions. The environmental chamber
364 presented in this study provides the possibility of simultaneous controlling/measuring both the
365 atmospheric and soil conditions: the air conditions were controlled (see Fig. 4, Fig. 5 and Fig.
366 8) and soil parameters were monitored simultaneously (see Fig. 6, Fig. 7, Fig. 9 and Fig. 11).
367 In addition, the attempt of the suction measurement suction in the zone near soil surface (see
368 Fig. 11) was also successful, which is, to the authors' knowledge, important and original
369 results. On the other hand, this chamber has also the functions of the tunnel system developed

370 by Yamanaka et al. (1997) and Yamanaka et al. (2004).

371

372 As far as the thickness of the soil column is concerned, previous studies (e.g., Ta et al. 2010;
373 Cui et al. 2013) showed that only the zone close to the soil surface is subjected to the effect of
374 evaporation. For this reason, the thickness of the soil column studied in the present work was
375 reduced to 300 mm. Furthermore, the sensors used for volumetric water content and soil
376 suction measurements were installed mainly in the near surface zone.

377

378 The soil water evaporation is an energy-consumption process. The main source of energy in
379 this experiment is the hot air circulated above the soil surface: the constant air rate and the
380 high inlet temperature (see Fig. 5) defined the energy for soil water evaporation. Therefore, at
381 the beginning of evaporation (i.e., the first six days), the soil water evaporation consumed a
382 lot of energy with a high evaporation rate (see Fig. 14), thereby, the air temperature increased
383 at a low rate (see Fig. 4). With the decrease of evaporation rate, the energy consumed by
384 water evaporation gradually decreased, resulting in air temperature increase at a high rate
385 after six days. On the other hand, the difference between the inlet and outlet air temperature
386 also shows that the soil water evaporation consumed energy from air. It should be noted that
387 the high temperature of 200 °C at the heating pipe generated a temperature of 47 °C at the
388 inlet and resulted in a temperature range from 24 °C to 32 °C in the chamber. This
389 temperature range is quite usual in France (Cui and Zornberg 2008).

390

391 The soil temperature change is an indicator of the energy (heat) change of soil during

392 evaporation. Figure 6 shows that the soil temperature increased as the air temperature (see Fig.
393 4) was rising, indicating that the soil was heated by hot air and the energy for water
394 evaporation was from the hot air. Furthermore, as evaporation is a progress of energy loss, the
395 temperature gradient in the soil surface zone (25-mm depth) is larger than in other depths.
396 This explains why evaporation is often limited to the near surface zone. Note that the soil
397 surface temperature measured by infrared thermometer in this study is more accurate than that
398 by sensors buried at the soil surface (e.g., Aluwihare and Watanabe 2003).

399

400 It can be noted in Fig. 7 that the air temperature in the zone close to the cover of chamber was
401 slightly lower than in the middle-height of the air part. This phenomenon suggests that heat
402 exchange existed between the environmental chamber and the laboratory ambiance. Therefore,
403 when estimating the soil water evaporation in the chamber, the energy balance method can not
404 be used. Regarding the fluctuation of soil temperature (about 0.5 °C) in deeper levels, it can
405 also be attributed to the influence of ambient temperature. Indeed, the temperature sensors
406 were buried at various distances from the chamber's wall (from 100 mm to 300 mm) and the
407 laboratory temperature effect is expected to be different.

408

409 For the air relative humidity (see Fig. 8), its decrease inside the chamber suggests that the
410 total water loss progressed (i.e., drying process) in the chamber. The relative humidity in the
411 chamber was not affected by the ambient one, showing that the good performance of the
412 chamber in controlling the air relative humidity; in other words, the ventilated part above the
413 soil surface was sealed efficiently and the water evaporated from soil was completely

414 transported to the outlet of chamber during the test. Thus, the calculation of evaporation based
415 on the measurements of the temperature and relative humidity at the inlet and outlet is reliable.
416 The similar value of relative humidity at different positions of chamber (e.g., 50-mm height,
417 275-mm height and outlet) confirms the homogeneity of relative humidity in the chamber.
418 The large gap of relative humidity between the inlet and outlet shows the effect of evaporation
419 in terms of supplying water vapor to the air.

420

421 The soil volumetric water content is an important indicator of water loss during evaporation.
422 The evolution of volumetric water content (see Fig. 9, Fig. 10(b)) shows a clear decline in the
423 near surface zone (i.e., within 60-mm depth). This justifies the denser disposition adopted for
424 the water content sensors in the near surface zone because it allows the water content profile
425 to be well defined in this zone. The water content decline during the first six days corresponds
426 to the initiation stage of evaporation (see Fig. 9, Fig. 10(a)) as reported by Wythers et al.
427 (1999). In this stage, the evaporation rate is high and the quantity of water consumed is large.
428 This explains the quick decline observed for the first six days. Afterwards, with the decrease
429 of evaporation rate due to the increasing suction in the soil (see Fig. 14), the water content
430 decrease was slowed down.

431

432 The measurement of matric suction near the soil surface using high-capacity tensiometer was
433 successful. If the volumetric water content increased linearly with depth in the near surface
434 zone (Fig. 10(a)), it is not the case for the suction which varied non-linearly with depth in this
435 zone, as indicated by the water retention curve in Fig. 13. Thereby, the measurement of soil

436 suction on soil surface is essential because we cannot estimate it by simple extrapolation. On
437 the other side, soil suction on soil surface is a key parameter in the determination of soil water
438 evaporation.

439

440 Regarding the evaporation rate (Fig. 14), it was decreasing during the test, showing three
441 distinct evaporation stages: constant-rate stage (from $t = 0$ day to $t = 6$ days), falling-rate stage
442 (from $t = 6$ days to $t = 10$ days) and low-rate stage (after $t = 10$ days), as also observed by Idso
443 et al. (1974) and Hillel (2004). This evaporation process resulted from the following
444 conditions:

445 (1) a continuous supply of heat by the hot air;

446 (2) a vapor pressure gradient between the soil surface and air - this gradient is reflected by the
447 air relative humidity gradient above the soil surface (see Fig. 8);

448 (3) a continuous supply of water from the tank outside the chamber.

449

450 According to the water balance during soil water evaporation, the cumulative evaporation
451 calculated by Method 1 should be equal to that by Method 2. However, Figure 15 shows that
452 at the end of test, the cumulative evaporation calculated by Method 1 is less than Method 2:
453 20.4 mm against 32.2 mm. This could be attributed to the presence of trapped air in the gravel
454 layer. During evaporation, the air bubbles dissipated and water could occupy the space
455 initially occupied by air, leading thereby to water flow to the chamber from the water tank. In
456 other words, this quantity of water just entered the gravel layer but not necessarily the soil
457 layer. As a result, the cumulative evaporation from Method 1 is close to that from the

458 cumulative changes of water content (i.e., 24.5 mm).

459

460 **Conclusion**

461 A large-scale environmental chamber was developed in order to study the soil water
462 evaporation process. The atmospheric conditions (air rate, relative humidity and temperature)
463 were controlled and monitored. The soil column was instrumented by various sensors for
464 measuring matric suction, volumetric water content and temperature. An evaporation test was
465 performed on the Fontainebleau sand to verify the relevance of the setup developed. The
466 following conclusions can be drawn:

467

468 The air temperature in the chamber was found to increase after six days, showing that with the
469 decrease of evaporation rate due to the soil suction increase, the energy consumed was
470 decreased, giving rise to air temperature increase.

471

472 The soil temperature was found to increase, indicating that the soil was heated by hot air and
473 the energy for water evaporation was from the hot air. In addition, as evaporation is a progress
474 of energy loss, the temperature gradient in the soil surface zone is larger than in deeper levels.

475

476 The temperature in the chamber was affected by the laboratory environment. But the relative
477 humidity in the chamber was not affected by the relative humidity of the laboratory - This
478 validated the method of actual evaporation determination based on the inlet and outlet relative
479 humidity values.

480

481 The evolution of volumetric water content showed significant changes of water content in the
482 near surface zone (within 60-mm depth). This justifies the denser disposition adopted for the
483 water content sensors in the near surface zone on the one hand, and the choice of a limited
484 height (300 mm) for the soil column on the other hand.

485

486 The attempt of near soil surface suction measurement by high-capacity tensiometer was
487 successful. This measurement is, to the authors' knowledge, original results. These results are
488 important since the soil surface suction is a key parameter in the determination of soil water
489 evaporation.

490

491 The relevant data obtained allowed the determination of actual evaporation rate and the water
492 retention curve. They also show the performance of the environmental chamber developed in
493 studying soil water evaporation. Moreover, they can be used in further theoretical
494 development for soil-atmosphere interaction investigation.

495

496 *Acknowledgments*

497 The authors are grateful to the support of China Scholarship Council (CSC).

498

499 **References**

500 Aluwihare, S. and Watanabe, K., 2003, "Measurement of Evaporation on Bare Soil and
501 Estimating Surface Resistance," *J. Environ. Eng.*, Vol. 129, No. 12, pp. 1157-1168.

502 Bathurst, R. J., Ho, A. F., and Siemens, G., 2007, "A Column Apparatus for Investigation of

503 1-D Unsaturated-Saturated Response of Sand-Geotextile Systems,” *Geotech. Test. J.*, Vol.
504 30, No. 6, pp. 433-441.

505 Bathurst, R. J., Siemens, G., and Ho, A. F., 2009, “Experimental Investigation of Infiltration
506 Ponding in One-Dimensional Sand-Geotextile Columns,” *Geosynth. Int.*, Vol. 16, No. 3,
507 pp. 158-172.

508 Benli, B., Kodal, S., Ilbeyi, A., and Ustun, H., 2006, “Determination of Evapotranspiration
509 and Basal Crop Coefficient of Alfalfa with a Weighing Lysimeter,” *Agr. Water Manage.*,
510 Vol. 81, No. 3, pp. 358-370.

511 Benson, C., Abichou, T., Albright, W., Gee, G., and Roesler, A., 2001, “Field Evaluation of
512 Alternative Earthen Final Covers,” *Int. J. Phytoremediat.*, Vol. 3, No. 1, pp. 105-127.

513 Blight, D. E., 1997, “Interactions Between the Atmosphere and the Earth,” *Géotechnique*, Vol.
514 47, No. 4, pp. 715-767.

515 Boast, C. W. and Robertson, T. M., 1982, “A ‘Micro-Lysimeter’ Method for Determining
516 Evaporation from Bare Soil: Description and Laboratory Evaluation,” *Soil Sci. Soc. Am. J.*,
517 Vol. 46, No. 4, pp. 689-696.

518 Bonachela, S., Orgaz, F., Villalobos, F. J., and Fereres, E., 1999, “Measurement and
519 Simulation of Evaporation from Soil in Olive Orchards,” *Irrig. Sci.*, Vol. 18, No. 4, pp.
520 205-211.

521 Corti, T., Muccione, V., Köllner-Heck, P., Bresch, D., and Seneviratne, S. I., 2009,
522 “Simulating Past Droughts and Associated Building Damages in France,” *Hydrol. Earth*
523 *Syst. Sci.*, Vol. 13, No. 9, pp. 1739-1747.

524 Corti, T., Wüest, M., Bresch, D., and Seneviratne, S. I., 2011, “Drought-Induced Building
525 Damages from Simulations at Regional Scale,” *Nat. Hazards Earth Syst. Sci.*, Vol. 11, No.
526 12, pp. 3335-3342.

527 Cui, Y. J. and Zornberg, J. G., 2008, “Water Balance and Evapotranspiration Monitoring in
528 Geotechnical and Geoenvironmental Engineering,” *Geotech. Geol. Eng.*, Vol. 26, No. 6,
529 pp. 783-798.

530 Cui, Y. J., Tang, A. M., Mantho, A. T., and De Laure, E., 2008, “Monitoring Field Soil
531 Suction Using a Miniature Tensiometer,” *Geotech. Test. J.*, Vol. 31, No. 1, pp. 95-100.

532 Cui, Y. J., Ta, A. N., Hemmati, S., Tang, A. M., and Gatmiri, B., 2013, “Experimental and

533 Numerical Investigation of Soil-Atmosphere Interaction,” *Eng. Geol.*, In Press.

534 Daamen, C. C. and Simmonds, L. P., 1996, “Measurement of Evaporation from Bare Soil and
535 its Estimation Using Surface Resistance,” *Water Resour. Res.*, Vol. 32, No. 5, pp.
536 1393-1402.

537 Delfosse-Ribay, E., Djeran-Maigre, I., Cabrillac, R., and Gouvenot, D., 2004, “Shear
538 Modulus and Damping Ratio of Grouted Sand,” *Soil Dyn. Earthq. Eng.*, Vol. 24, No. 6, pp.
539 461-471.

540 Fredlund, D. G. and Xing, A., 1994, “Equations for the Soil-Water Characteristic Curve,”
541 *Can. Geotech. J.*, Vol. 31, No. 4, pp. 521-532.

542 Fu, G., Liu C., Chen, S., and Hong, J., 2004, “Investigating the Conversion Coefficients for
543 Free Water Surface Evaporation of Different Evaporation Pans,” *Hydrol. Process*, Vol. 18,
544 No. 12, pp. 2247-2262.

545 Fu, G., Charles, S. P., and Yu, J., 2009, “A Critical Overview of Pan Evaporation Trends over
546 the Last 50 Years,” *Clim. Change*, Vol. 97, No. 1-2, pp. 193-214.

547 Hillel, D., 2004, *Introduction to Environmental Soil Physics*, Elsevier Academic Press,
548 Amsterdam, p. 494.

549 Idso, S. B., Reginato, R. J., Jackson, R. D., Kimball, B. A., and Nakayama, F. S., 1974, “The
550 Three Stages of Drying of a Field Soil,” *Soil Sci. Soc. Am. J.*, Vol. 38, No. 5, pp. 831-837.

551 Kohsiek, W., 1981, “A Rapid-Circulation Evaporation Chamber for Measuring Bulk Stomatal
552 Resistance,” *J. Appl. Meteor.*, Vol. 20, No. 1, pp. 42-52.

553 Komatsu, T. S., 2003, “Toward a Robust Phenomenological Expression of Evaporation
554 Efficiency for Unsaturated Soil Surfaces,” *J. Appl. Meteor.*, Vol. 42, No. 9, pp. 1330-1334.

555 Kondo, J., Saigusa, N., and Sato, T., 1990, “A Parameterization of Evaporation from Bare
556 Soil Surfaces,” *J. Appl. Meteor.*, Vol. 29, No. 5, pp. 385-389.

557 Kondo, J., Saigusa, N., and Sato, T., 1992, “A Model and Experimental Study of Evaporation
558 from Bare-Soil Surfaces,” *J. Appl. Meteor.*, Vol. 31, No. 3, pp. 304-312.

559 Lal, R. and Shukla, M. K., 2004, *Principles of Soil Physics*, Marcel Dekker, New York, p.
560 716.

561 Li, J. H. and Zhang, L. M., 2011, “Study of Desiccation Crack Initiation and Development at
562 Ground Surface,” *Eng. Geol.*, Vol. 123, No. 4, pp. 347-358.

- 563 Liu, C., Zhang, X., and Zhang, Y., 2002, "Determination of Daily Evaporation and
564 Evapotranspiration of Winter Wheat and Maize by Large-Scale Weighing Lysimeter and
565 Micro-Lysimeter," *Agr. Forest Meteorol.*, Vol. 111, No. 2, pp. 109-120.
- 566 McCartney, J. S. and Zornberg, J. G., 2010, "Effects of Infiltration and Evaporation on
567 Geosynthetic Capillary Barrier Performance," *Can. Geotech. J.*, Vol. 47, No. 11, pp.
568 1201-1213.
- 569 Mohamed, A. A., Sasaki, T., and Watanabe, K., 2000, "Solute Transport Through
570 Unsaturated Soil Due to Evaporation," *J. Environ. Eng.*, Vol. 126, No. 9, pp. 842-848.
- 571 Plauborg, F., 1995, "Evaporation from Bare Soil in a Temperate Humid Climate
572 -Measurement Using Micro-Lysimeters and Time Domain Reflectometry," *Agr. Forest
573 Meteorol.*, Vol. 76, No. 1, pp. 1-17.
- 574 Qiu, G. Y., Yano, T., and Momii, K., 1998, "An Improved Methodology to Measure
575 Evaporation from Bare Soil Based on Comparison of Surface Temperature with a Dry
576 Soil Surface," *J. Hydrol.*, Vol. 210, No. 1-4, pp. 93-105.
- 577 Singh, V. P. and Xu, C. Y., 1997, "Evaluation and Generalization of 13 Mass-Transfer
578 Equations for Determining Free Water Evaporation," *Hydrol. Process.*, Vol. 11, No. 3, pp.
579 311-323.
- 580 Stormont, J. C. and Anderson, C. E., 1999, "Capillary Barrier Effect from Underlying Coarser
581 Soil Layer," *J. Geotech. Geoenviron. Eng.*, Vol. 125, No. 8, pp. 641-648.
- 582 Ta, A. N., Tang, A. M., Cui, Y. J., and Thiriat, J., 2010, "An Environmental Chamber for
583 Studying the Soil-Atmosphere Interaction," *Unsaturated soils, Proceedings of the Fifth
584 International Conference on Unsaturated Soils*, Alonso and Gens, Eds., Barcelona, Spain,
585 September 6-8, 2010, Taylor & Francis Group, London, pp. 1141-1146.
- 586 Tang, A. M., Ta, A. N., Cui, Y. J., and Thiriat, J., 2009, "Development of a Large-Scale
587 Infiltration Tank for Determination of the Hydraulic Properties of Expansive Clays,"
588 *Geotech. Test. J.*, Vol. 32, No. 5, pp. 385-396.
- 589 Tang, A. M., Cui, Y. J., Qian, L. X., Delage, P., and Ye, W. M., 2010, "Calibration of the
590 Osmotic Technique of Controlling Suction with Respect to Temperature Using a Miniature
591 Tensiometer," *Can. Geotech. J.*, Vol. 47, No. 3, pp. 359-365.
- 592 van de Griend, A. A. and Owe, M., 1994, "Bare Soil Surface Resistance to Evaporation by

593 Vapor Diffusion Under Semiarid Conditions,” *Water Resour. Res.*, Vol. 30, No. 2, pp.
594 181-188.

595 Wang, W. Z., 2006, “Wind Tunnel Experiments on Bare Soil Evaporation,” MSc. thesis,
596 National Central University, Taiwan, p. 82.

597 Wang, H. and Simmonds, L. P., 1997, “Measurement and Simulation of Evaporation from a
598 Bare Soil,” *J. Environ. Sci.*, Vol. 9, No. 4, pp. 446-453.

599 Wilson, G. W., Fredlund, D. G., and Barbour, S. L., 1994, “Coupled Soil-Atmosphere
600 Modelling for Soil Evaporation,” *Can. Geotech. J.*, Vol. 31, No. 2, pp. 151-161.

601 Wilson, G. W., Fredlund, D. G., and Barbour, S. L., 1997, “The Effect of Soil Suction on
602 Evaporative Fluxes from Soil Surfaces,” *Can. Geotech. J.*, Vol. 34, No. 1, pp. 145-155.

603 Wythers, K. R., Lauenroth, W. K., and Paruelo, J. M., 1999, “Bare-Soil Evaporation Under
604 Semiarid Field Conditions,” *Soil Sci. Soc. Am. J.*, Vol. 63, No. 5, pp. 1341-1349.

605 Yamanaka, T., Takeda, A., and Sugita, F., 1997, “A Modified Surface-Resistance Approach
606 for Representing Bare-Soil Evaporation: Wind Tunnel Experiments Under Various
607 Atmospheric Conditions,” *Water Resour. Res.*, Vol. 33, No. 9, pp. 2117-2128.

608 Yamanaka, T., Inoue, M., and Kaihotsu, I., 2004, “Effects of Gravel Mulch on Water Vapor
609 Transfer Above and Below the Soil Surface,” *Agr. Water Manage.*, Vol. 67, No. 2, pp.
610 145-155.

611 Yanful, E. K. and Choo, L. P., 1997, “Measurement of Evaporation Fluxes from Candidate
612 Cover Soils,” *Can. Geotech. J.*, Vol. 34, No. 3, pp. 447-459.

613 Yanful, E. K., Mousavi, S. M., and Yang, M., 2003, “Modeling and Measurement of
614 Evaporation in Moisture-Retaining Soil Covers,” *Adv. Environ Res.*, Vol. 7, No. 4, pp.
615 783-801.

616 Yuge, K., Haraguchi, T., Nakano, Y., Kuroda, M., and Anan, M., 2005, “Quantification of
617 Soil Surface Evaporation Under Micro-Scale Advection in Drip-Irrigated Fields,” *Paddy
618 Water Environ.*, Vol. 3, No. 1, pp. 5-12.

619

620 **List of Tables**

621 TABLE 1. *The sensors used*

622

623 **List of Figures**

624 FIG. 1—*Sketch of the environmental chamber test system*

625 FIG. 2—*Schematic presentation of the environmental chamber:(a) Three-dimension view of environmental*

626 *chamber (in mm) and (b) schematic cross section of the environmental chamber (A-A)*

627 FIG. 3—*Photograph of the environmental chamber test system*

628 FIG. 4—*Evolutions of air temperature at different elevations*

629 FIG. 5—*Evolutions of air temperature at the inlet and outlet of chamber as well as in the laboratory*

630 FIG. 6—*Evolutions of soil temperature at different locations*

631 FIG. 7—*Profiles of air-soil temperature*

632 FIG. 8—*Evolutions of air relative humidity at different locations in the chamber as well as in the*

633 *laboratory*

634 FIG. 9—*Evolutions of volumetric water content at different depths*

635 FIG. 10—*Profiles of volumetric water content (a) and contour map (b) at different times*

636 FIG. 11—*Evolutions of soil matric suction at different depths*

637 FIG. 12—*Profiles of soil matric suction at different times*

638 FIG. 13—*Soil-water retention curve determined based on the measured suction and volumetric water*

639 *content values*

640 FIG. 14—*Evolutions of actual evaporation rate and suction gradient between soil surface and 77-mm*

641 *depth*

642 FIG. 15—*Comparison of cumulative evaporation determined by two different methods*

643

644

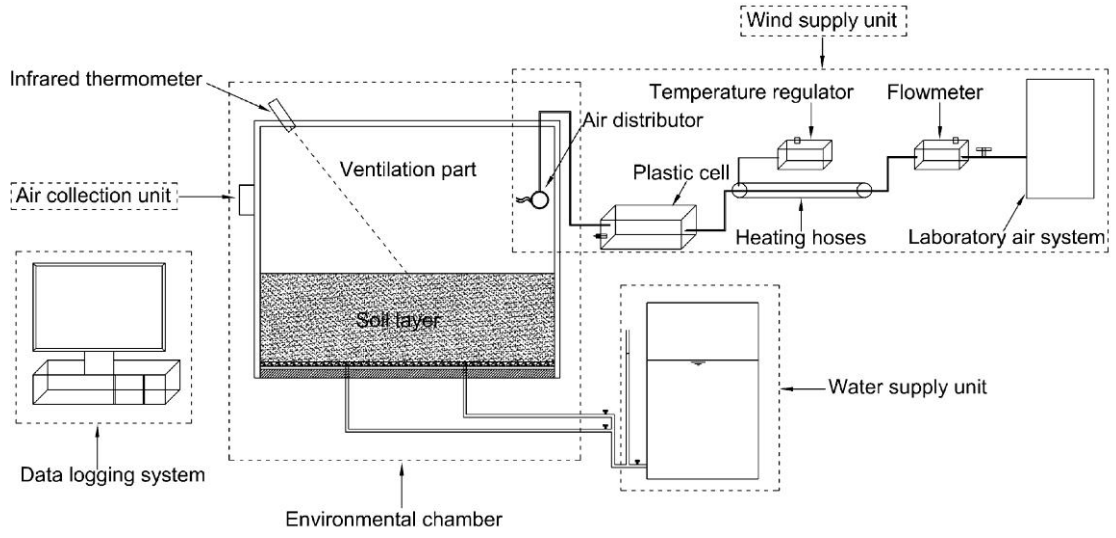
645 TABLE 1—*The sensors used*

Sensor	Manufacturer	Model	Parameter measured	Range	Accuracy	Number
High-capacity tensiometer	ENPC		Matric suction	0-1.5 MPa		5
Transmitter	Elcowa	T3111	Relative humidity	0-100 %	± 2.5 %	6
			Temperature	-30-150 °C	± 0.4 °C	
ThetaProbe	Delta-T	ML2x	Volumetric water content	0-100 %	± 1.0 %	5
Resistance temperature detectors	Correge	PT1000	Temperature	0-100 °C	± 0.3 °C	6
Thermistor	Radiospare	DO-35	Temperature	-40-250 °C	± 1.0 %	5
Infrared Thermometer	Calex	Pyropen-D	Temperature	-20-250 °C	± 1.0 %	1
Flowmeter	Kobold	MAS-3120	Air flow	0-500 L/min	± 1.5 % full scale	1

646

647

648



649

650 FIG. 1—Sketch of the environmental chamber test system

651

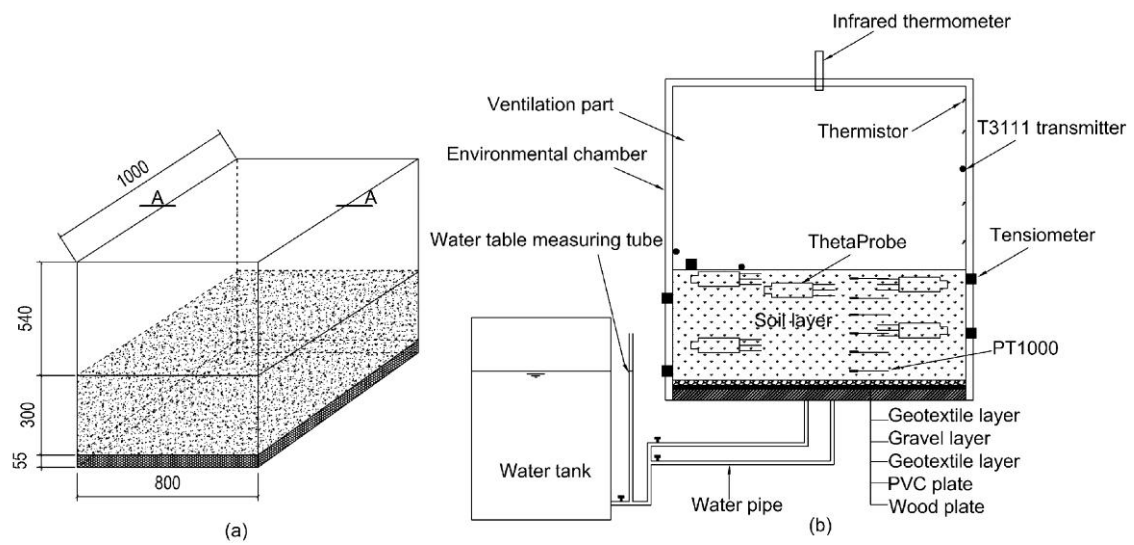


FIG. 2—Schematic presentation of the environmental chamber:(a) Three-dimension view of environmental chamber (in mm) and (b) schematic cross section of the environmental chamber (A-A)

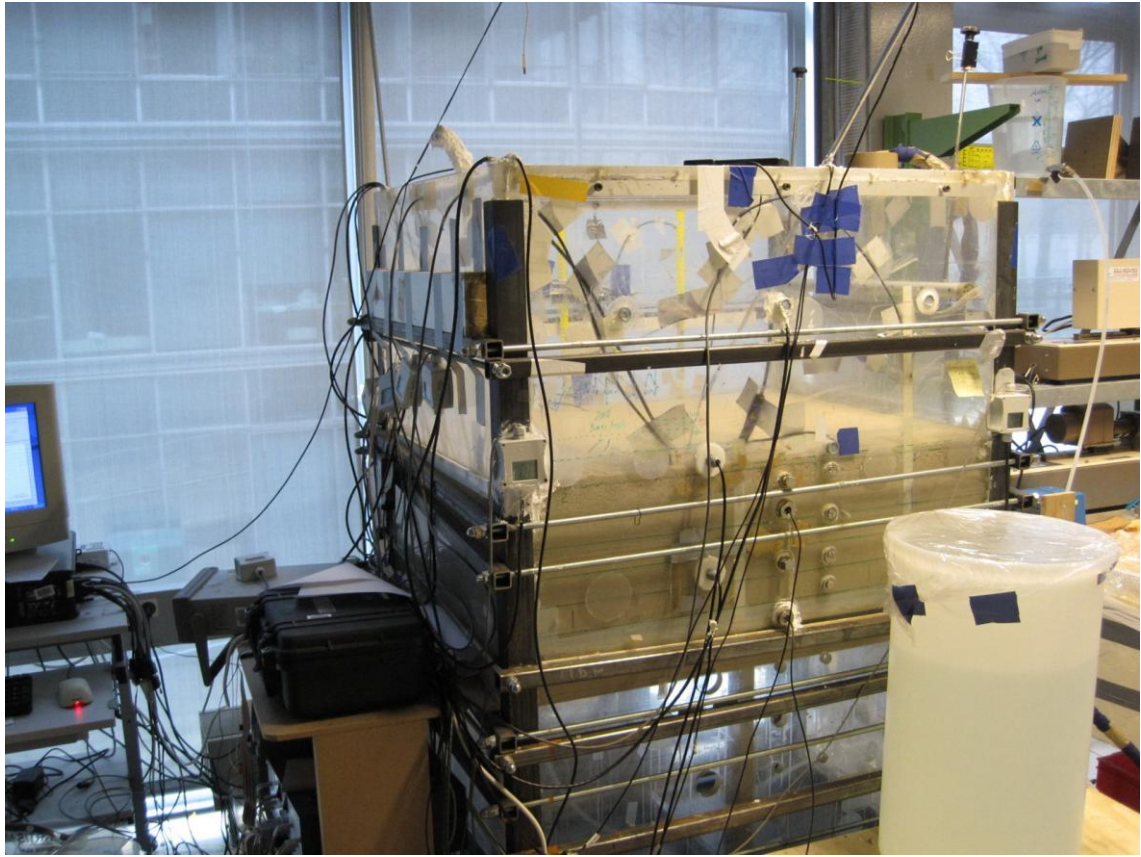


FIG. 3—*Photograph of the environmental chamber test system*

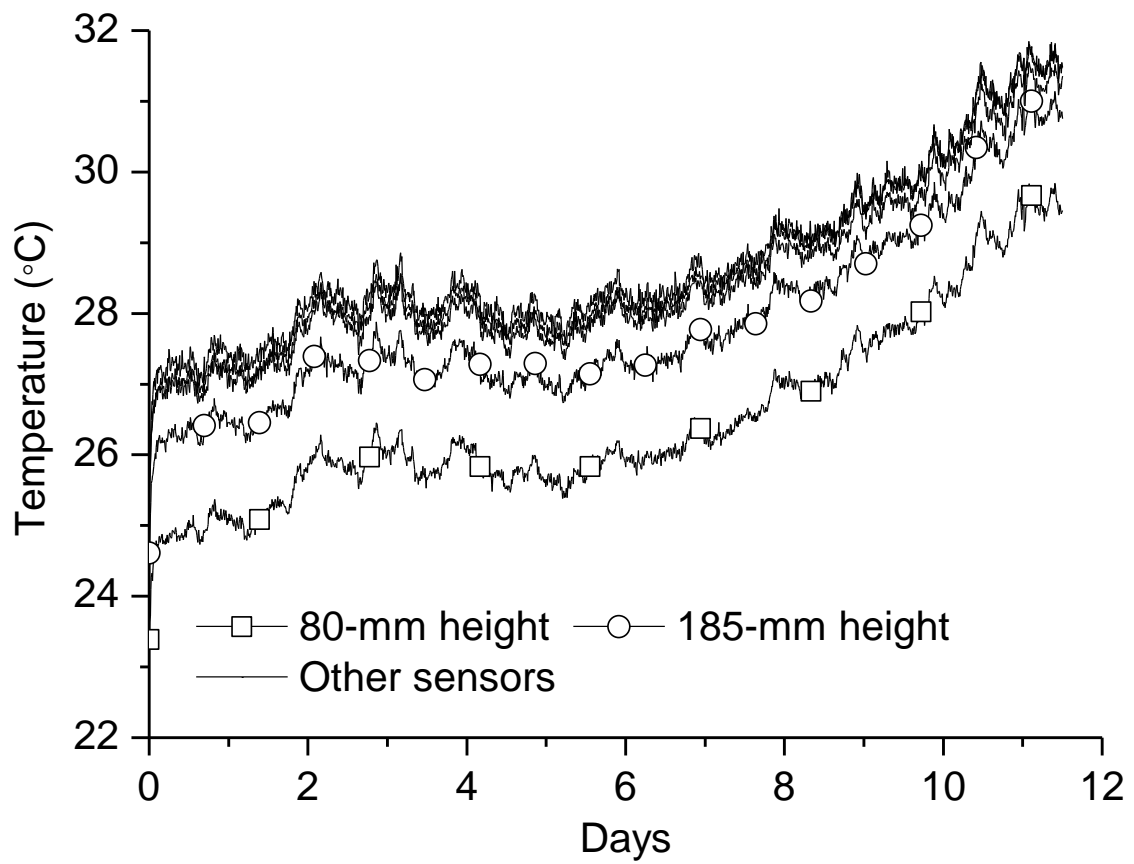


FIG. 4—Evolutions of air temperature at different elevations

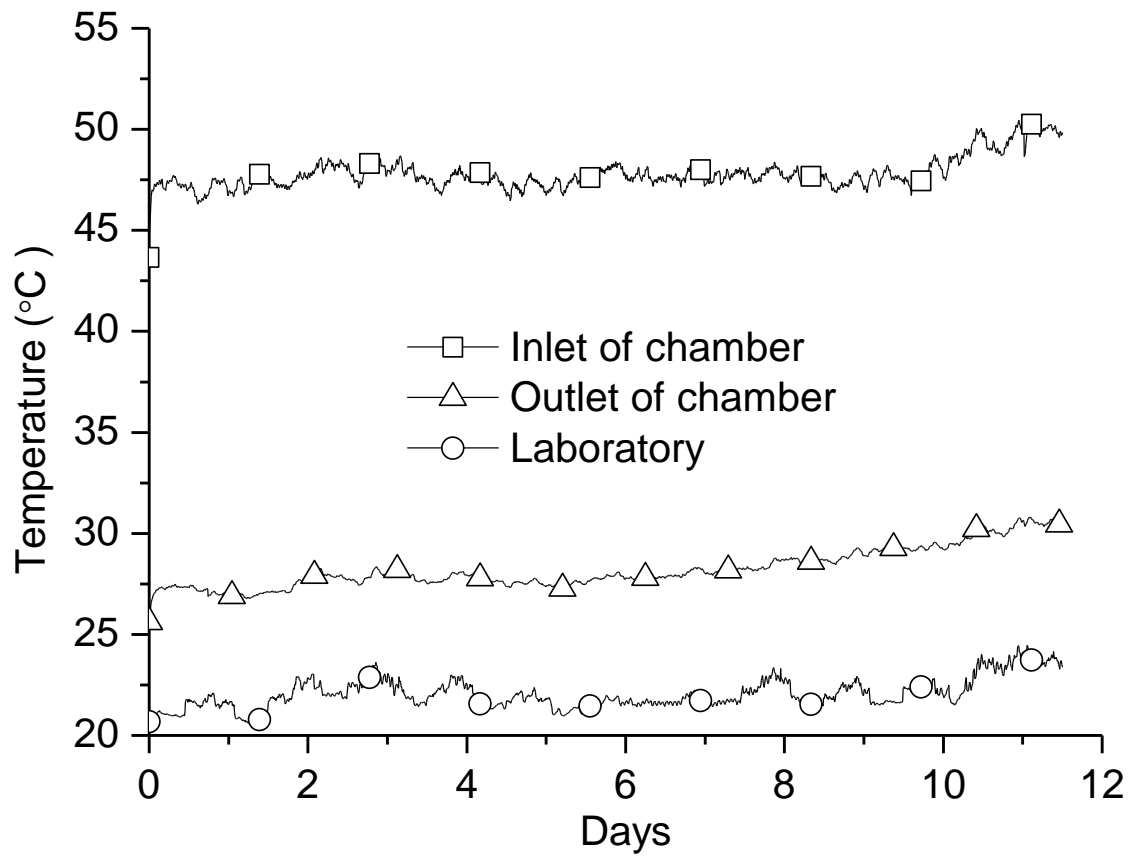


FIG. 5—Evolutions of air temperature at the inlet and outlet of chamber as well as in the laboratory

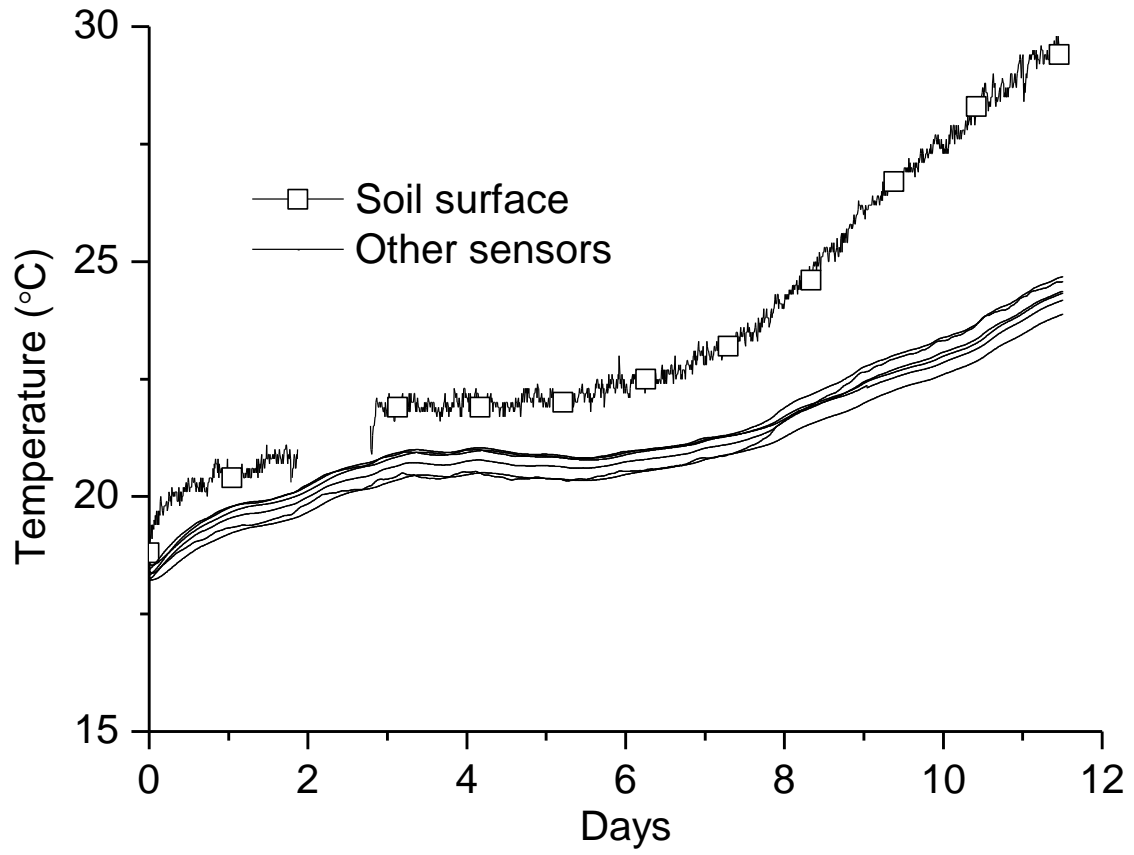


FIG. 6—Evolutions of soil temperature at different locations

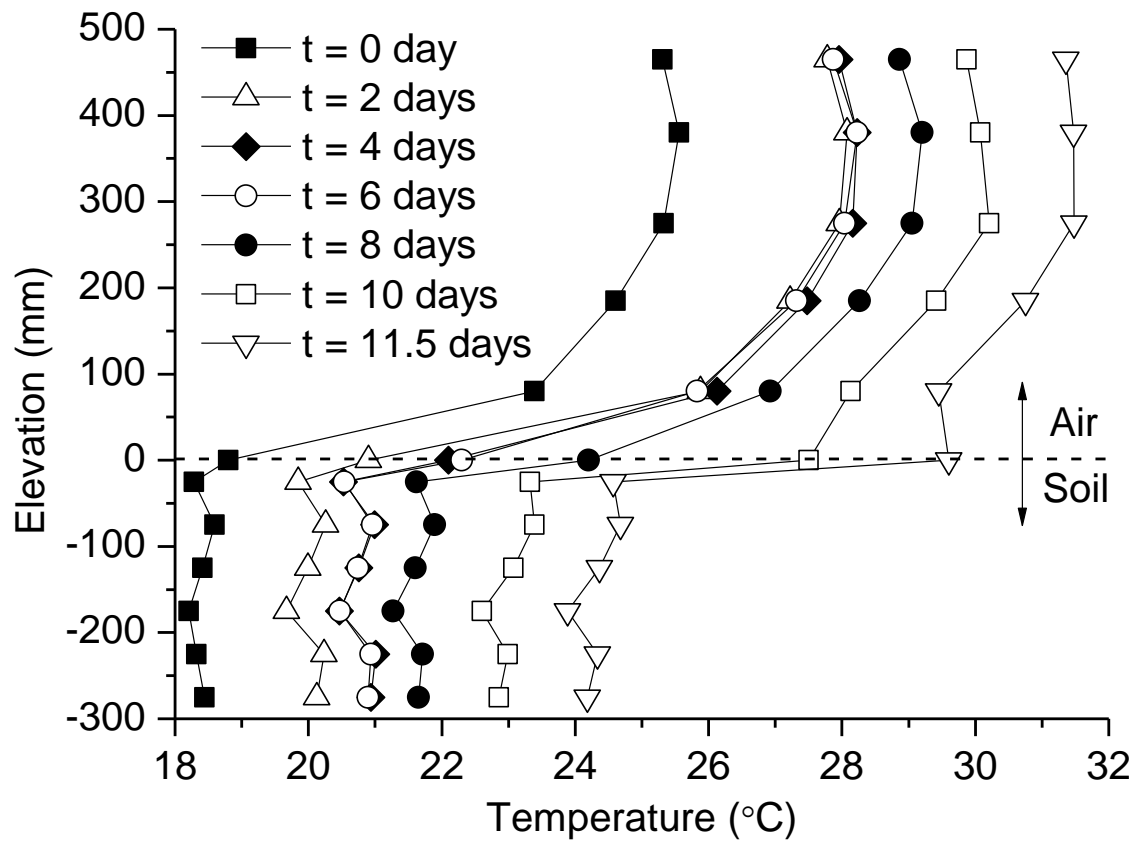


FIG. 7—Profiles of air-soil temperature

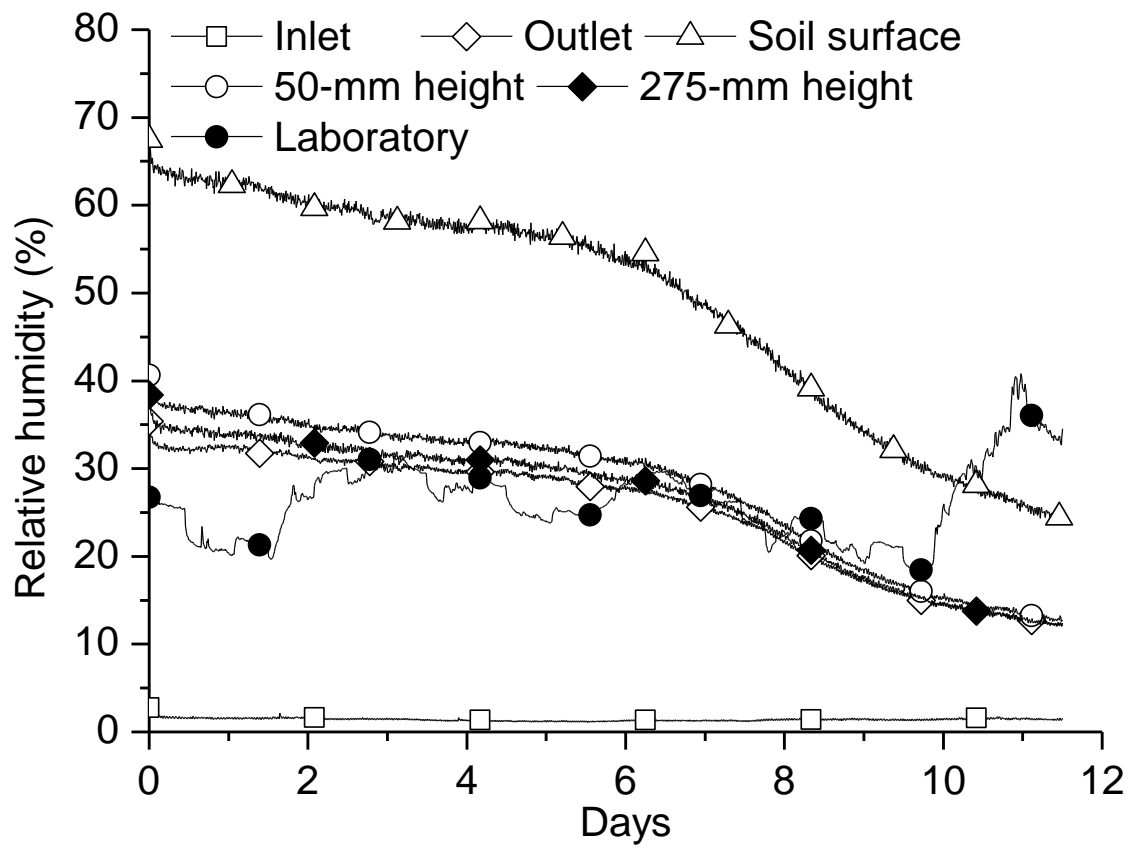


FIG. 8—Evolutions of air relative humidity at different locations in the chamber as well as in the laboratory

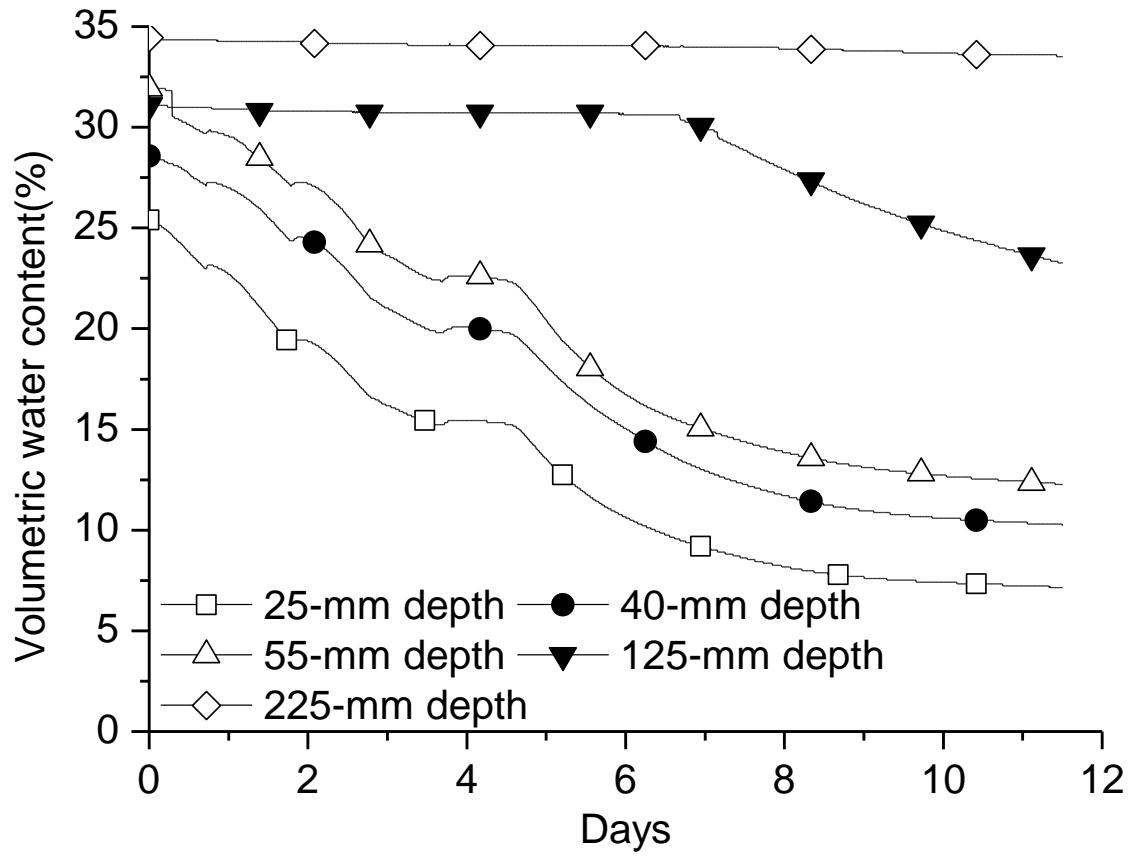


FIG. 9—Evolutions of volumetric water content at different depths

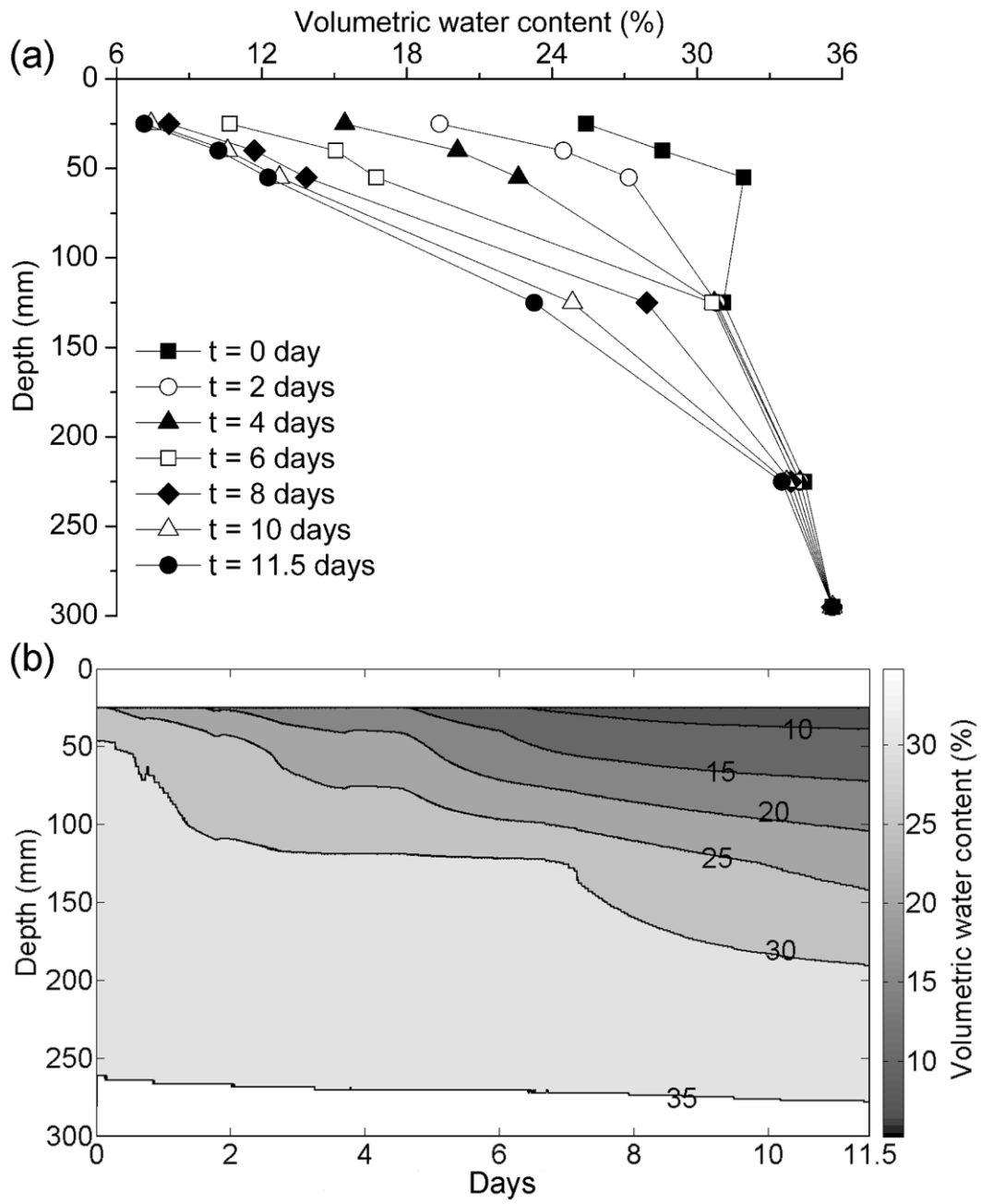


FIG. 10—Profiles of volumetric water content (a) and contour map (b) at different times

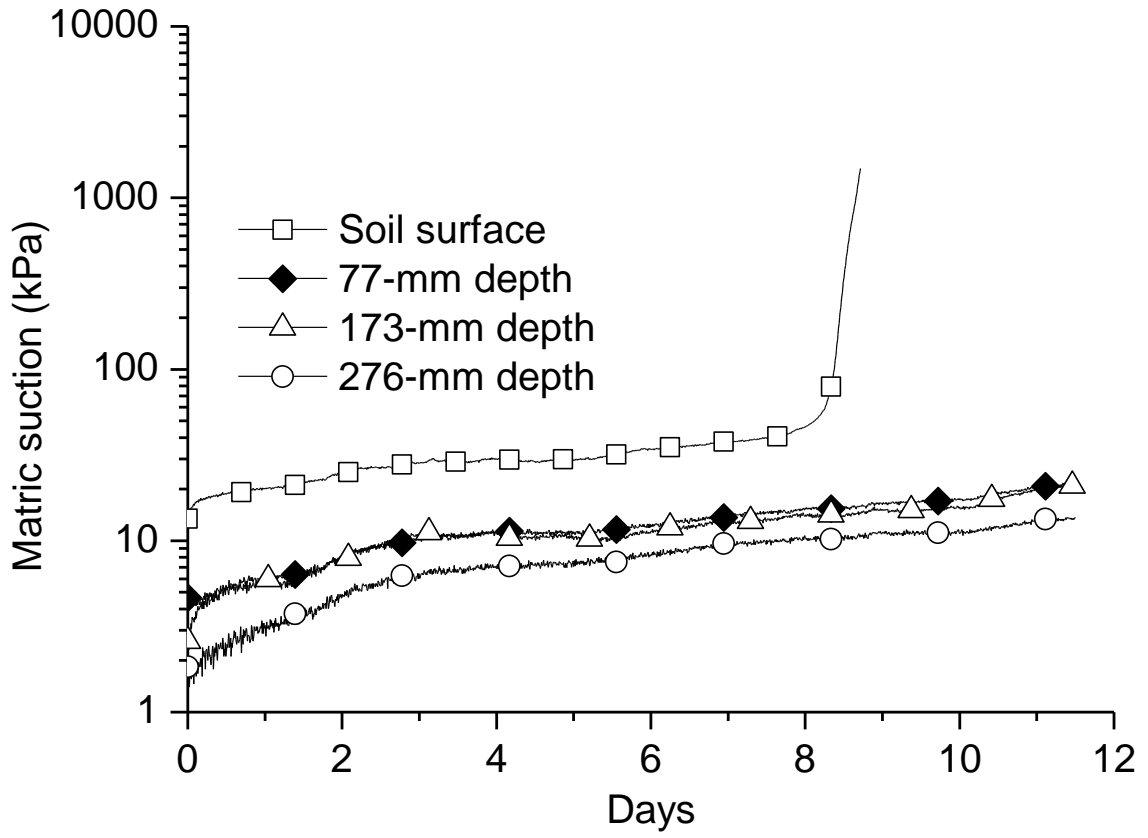


FIG. 11—Evolutions of soil matric suction at different depths

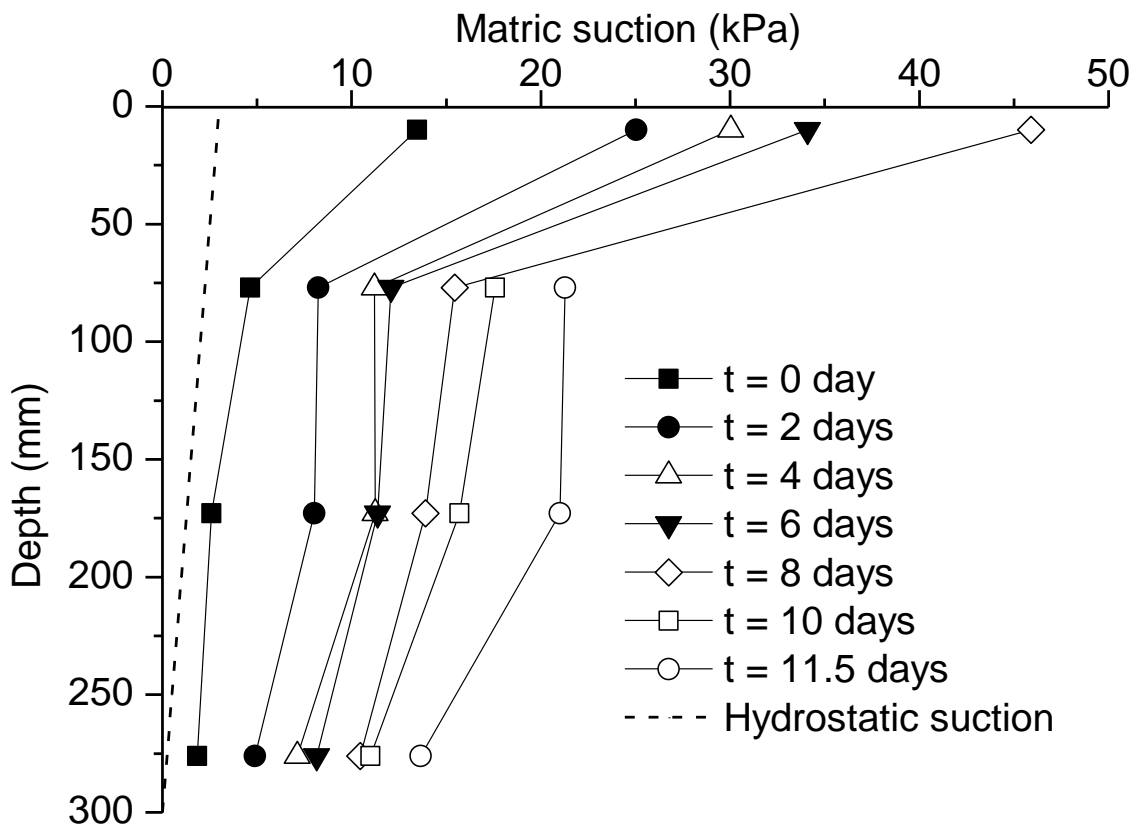


FIG. 12—Profiles of soil matric suction at different times

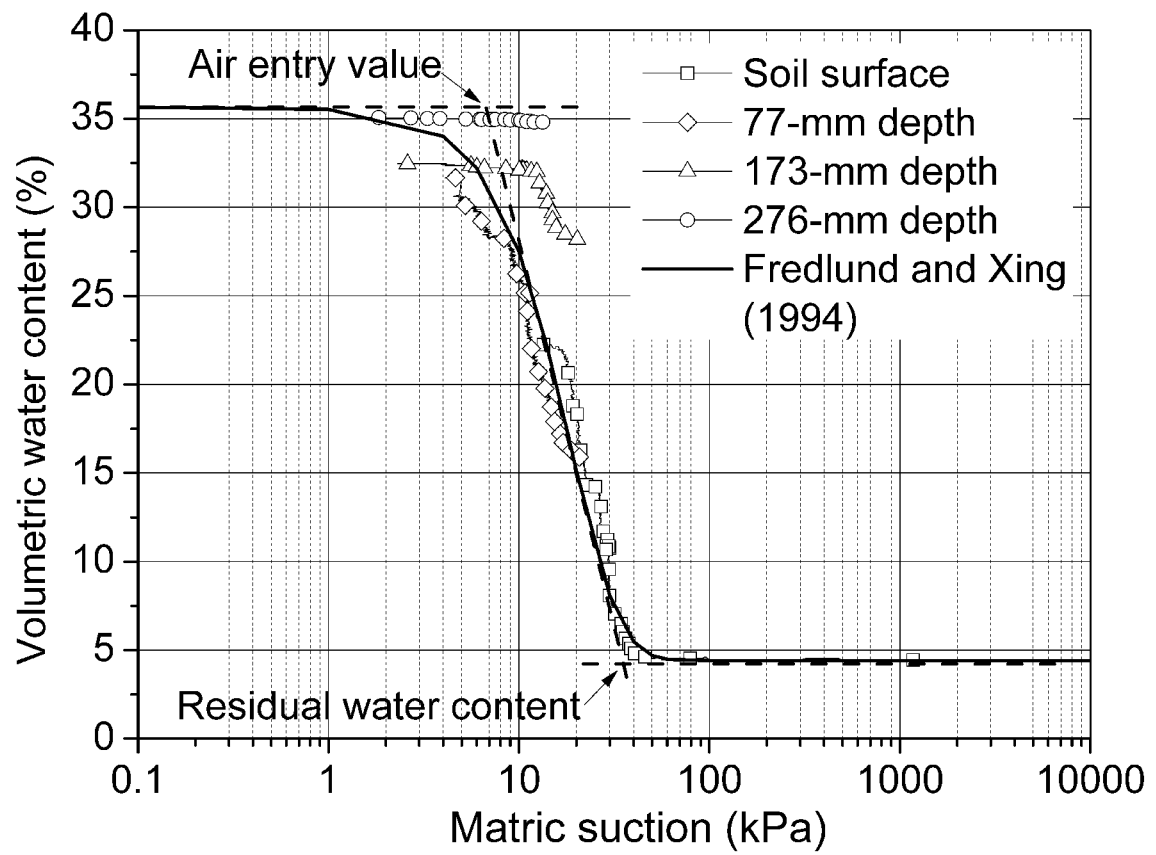


FIG. 13—Soil-water retention curve determined based on the measured suction and volumetric water content values

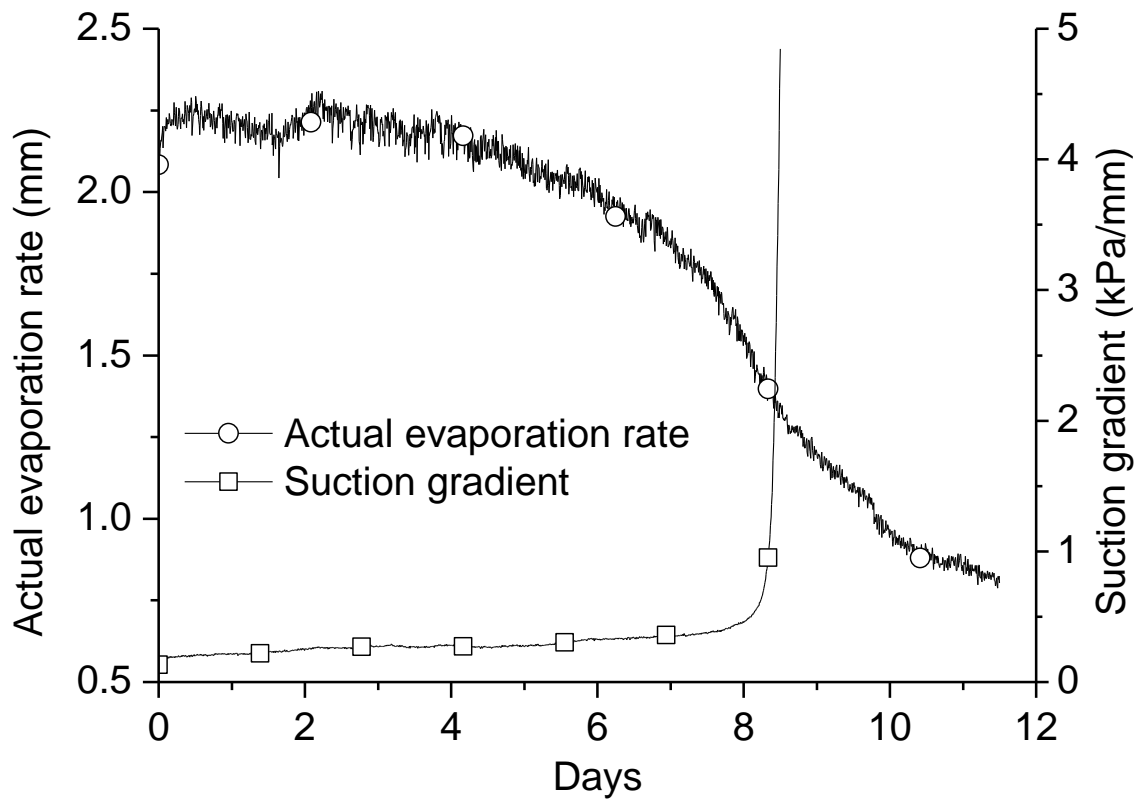


FIG. 14—Evolutions of actual evaporation rate and suction gradient between soil surface and 77-mm depth

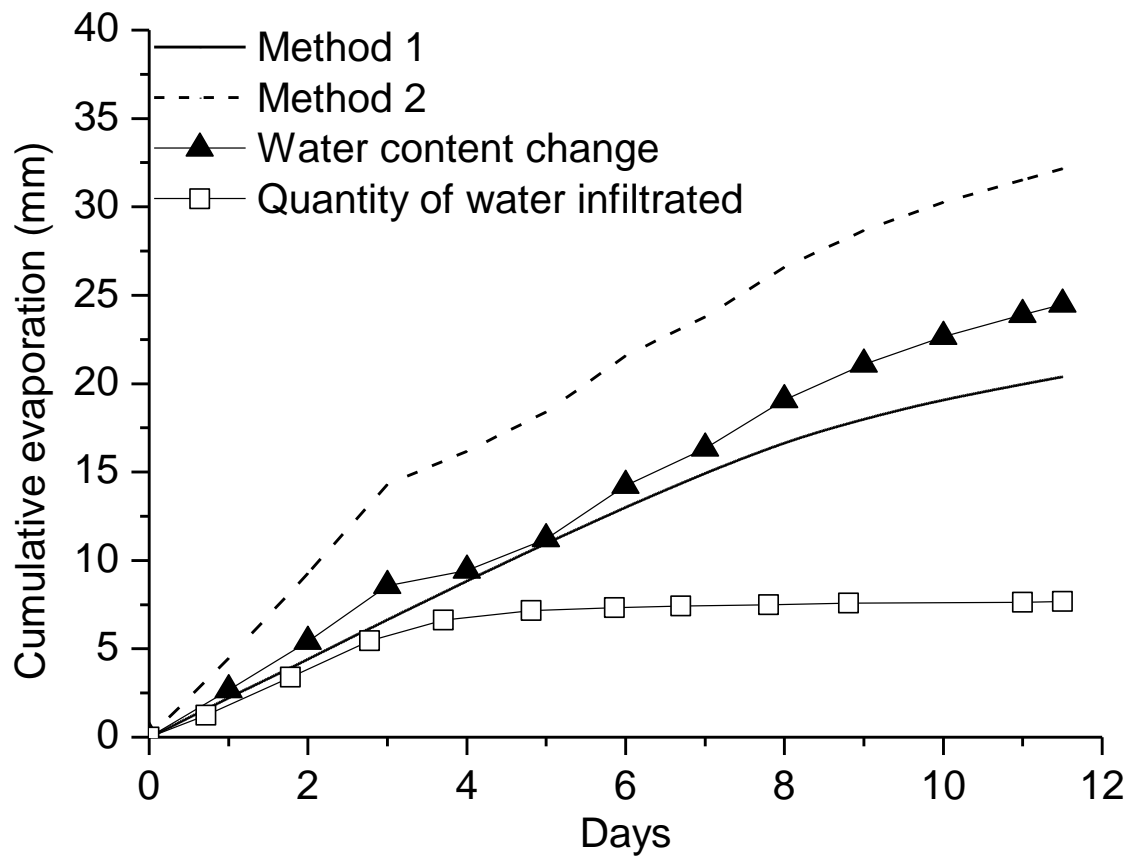


FIG. 15—Comparison of cumulative evaporation determined by two different methods